Agricultural Water Management 269 (2022) 107652

Contents lists available at ScienceDirect

Agricultural Water Management

journal homepage: www.elsevier.com/locate/agwat

Unravelling soil water dynamics in almond orchards characterized by soil-heterogeneity using electrical resistivity tomography

Daniela Vanella [a,*], Srinivasa Rao Peddinti [b], Isaya Kisekka [b]

[a] Dipartimento di Agricoltura, Alimentazione e Ambiente (Di3A), Università degli Studi di Catania, Via S. Sofia, 100, Catania 95123, Italy
[b] Department of Land Air & Water Resources, and Department of Biological and Agricultural Engineering, University of California Davis, Davis, CA 95616, USA

ARTICLE INFO

Keywords:
Soil-water variability
Precision irrigation
Almonds
Water management

ABSTRACT

Characterizing soil heterogeneity helps to improve the management of the natural resources (mainly water, nutrients and soil itself) at the farm level and enhances crop growth and relative yield sustainability. In this context, the geophysical monitoring based on direct current methods (such as the Electrical Resistivity Tomography, ERT) can help to detect the soil heterogeneity by exploring the soil water variability. ERT time-lapse surveys were carried out in almond orchards characterized by different soil types in terms of structure (i.e. layered, light and heavy soil profiles) and texture features (i.e. prevalently clay loam versus sandy clay loam). Specifically, two-dimensional ERT surveys were combined with the monitoring of multiple soil-plant-atmosphere factors, including the components of the surface energy balance using an eddy covariance system, the soil moisture and the plant water status measured using a neutron probe and pressure chamber measurements, respectively. The interpretation of the ERT results together with the ancillary data has provided spatially and temporally distributed information about the soil water processes that occurred within the almond root-zone during irrigation, allowing us to identify where the most root-water uptake occurs and the delineation of the irrigation wet bulbs under micro-irrigations conditions.

1. Introduction

Spatial heterogeneity of subsurface properties plays a pivotal role in governing plant health (De Benedetto et al., 2013). Understanding the role of soil heterogeneity is particularly important for sustaining agricultural production under limited, since it may affect the preferential flow through macro pores and cause water and/or nutrients flow and transport losses groundwater (Šimůnek et al., 2003). Furthermore, this aspect is crucial in marginal soils, such as the west side of the Sacramento Valley (California, USA). These marginal soils tend to have higher spatial variability in soil depth profile, texture, and structure. The variability of the soil factors influences the available water holding capacity, the fertility, and sometimes the salinity (and eventually sodicity) at the root zone level (Fulton et al., 2011). The heterogeneity of the soil physical and hydraulic properties is translated into greater orchard variability both in terms of canopy growth and crop production (Kisekka, 2021). In order to account for the natural variability of the soils in a parcel of land, the implementation of the so-called zone irrigation management is needed for helping the growers in the adoption of precision irrigation systems (Fulton et al., 2011).

In general, several biotic (e.g. roots distribution, root water uptake, soil organisms) and abiotic (e.g. soil structure and soil texture, soil aggregation and compaction, climatic condition) factors contribute to affect the soil heterogeneity (Vereecken et al., 2008). In irrigated agriculture, the dynamics of state variables, such as soil moisture (mainly driven by irrigation water supplies and precipitation), can be recognized as a *proxy* of soil heterogeneity and root activity response detection (Vereecken et al., 2016). Despite its critical importance, challenges remain in acquiring soil moisture information at appropriate spatial and temporal resolutions mainly because their evaluations typically depend on the scale of observation. Nowadays, a number of technologies and tools based on geophysical properties, such as electrical conductivity (inverse of the electrical resistivity, ER), can provide information on subsurface heterogeneity in terms of soil water flow changes (including near surface geophysics, remote and proximal sensing approaches, using platforms that range from aircraft to unmanned air vehicles).

Among these methods, near surface geophysics provides a multidimensional set of investigative methods for monitoring the subsurface dynamics at diverse scales (Binley et al., 2015). In general, the spatial range achievable from the available hydrogeophysical methods (such as,

* Corresponding author.
E-mail address: daniela.vanella@unict.it (D. Vanella).

https://doi.org/10.1016/j.agwat.2022.107652
Received 5 January 2022; Received in revised form 7 April 2022; Accepted 10 April 2022
Available online 20 April 2022

Table 1
Site-specific soil and plant characteristics of the almond orchards under study at the CAPEX ranch located near Corning, California.

Almond orchard #	Lat (°N), Long (°E)	Varieties-rootstocks	Tree spacing (m)	Soil type zone
C230#1	39.956,−122.245	Nonpareil-Peach	4.8	Layered
C230#2	39.956,−122.247			
C7#12	39.951,−122.267	Monterey-Peach	3.4	Heavy
C7#14	39.954,−122.265			
C6#9	39.956,−122.263	Butte-Marianna 2624		Light

electrical resistivity tomography, ERT; helicopter-borne frequency domain electromagnetic induction, FDEM; time domain electromagnetic, TDEM; towed, ground-based, transient electromagnetic system, tTEM; ground penetrating radar) is variable as function of the horizontal and vertical scales of investigation that each method is able to provide (ranging from 1 to 10,000 m for the horizontal extent and from 0.1 to 100 m for the depth of investigation). Thus, the choice of the appropriate method is dependent both on the given problem (target) and on the footprint of the geophysical measurement (Binley et al., 2015). Even if most applications only rely on a single geophysical survey at a given time, time-lapse geophysical surveys have greater capabilities to characterize the soil subsurface flow dynamics (Blanchy et al., 2020). A great compromise, in terms of lateral coverage and depth of investigation, is delivered by the so-called direct current methods based on ERT and ERI techniques (Binley, 2015; Binley and Kemna, 2005). These techniques, applied both in static and in time-lapse mode, are able to provide accurate information about the soil water spatial heterogeneity due to the flow and storage processes acting at the root-zone level, making such techniques relevant for soil-water-plant relationship related applications (Cassiani et al., 2015; Vanella et al., 2018, 2019).

Other indirect approaches have linked the crop water stress–related phenomena (e.g. identifying the crop vigor and the crop water status) for predicting soil heterogeneities information (Rudolph et al., 2015; Vereecken et al., 2012). However, more research is still needed to enhance our ability to link more directly the soil water status with the plant-water status response. To better address the issue, the integration of multiple methodologies for measuring the soil-water-plant atmosphere system can contribute to offering a more realistic picture of the soil water heterogeneities and their impact on agronomic practices such as precision irrigation management (Bellvert et al., 2021; Kisekka et al., 2021).

The main objective of this study was to evaluate the effect of soil heterogeneity characterized by variability in soil structure (i.e. layered, light and heavy soil profiles) and texture (i.e. prevalently clay loam versus sandy clay loam) on root zone soil water dynamics, active during irrigation cycles, in almond orchards using the ERT technique in time-lapse mode. Also, in order to link the soil and plant water status conditions multiple ground-based measurements (i.e. micro-meteorological, stem water potential and soil moisture measurements) were carried out at the same spatial and temporal scale as the ERT surveys.

Table 2
Details on the soil profile characteristics at the CAPEX ranch.

Soil profile types	Depth (cm)	Sand (%)	Clay (%)	Silt (%)	Hydraulic conductivity (mm/hr)
Layered Soil (Tehama silt loam)	0-5	69	15	16	28.8
	5-36	43	18	39	25.2
	36-64	42	20	38	25.2
	64-150	56	26	18	32.4
	150-183	40	23	37	21.6
Heavy Soil (Arbuckle fine loamy)	0–5	37	14	49	18.0
	5–36	35	17	48	18.0
	36–64	25	29	46	7.2
	64–150	32	24	44	18.0
	150 – 183	5	24	71	21.6
Light Soil (Arbuckle gravelly loam)	0–5	43	17	40	25.2
	5–36	43	18	39	25.2
	36–64	42	20	38	25.2
	64–150	56	26	18	32.4
	150 – 183	40	23	37	21.6

[1]UC Davis and USDA NRCS Soil Data Portal: https://casoilresource.lawr.ucdavis.edu/gmap/

Fig. 1. Overview of the study site, including the point locations used for the electrical resistivity tomography (ERT) surveys in the different almond blocks/soil management zones (Havy, Layered and Light soil) at CAPEX farm located near Corning, California. For interpretation of the references to colour in this figure legend, the reader is referred to the web version of this article.

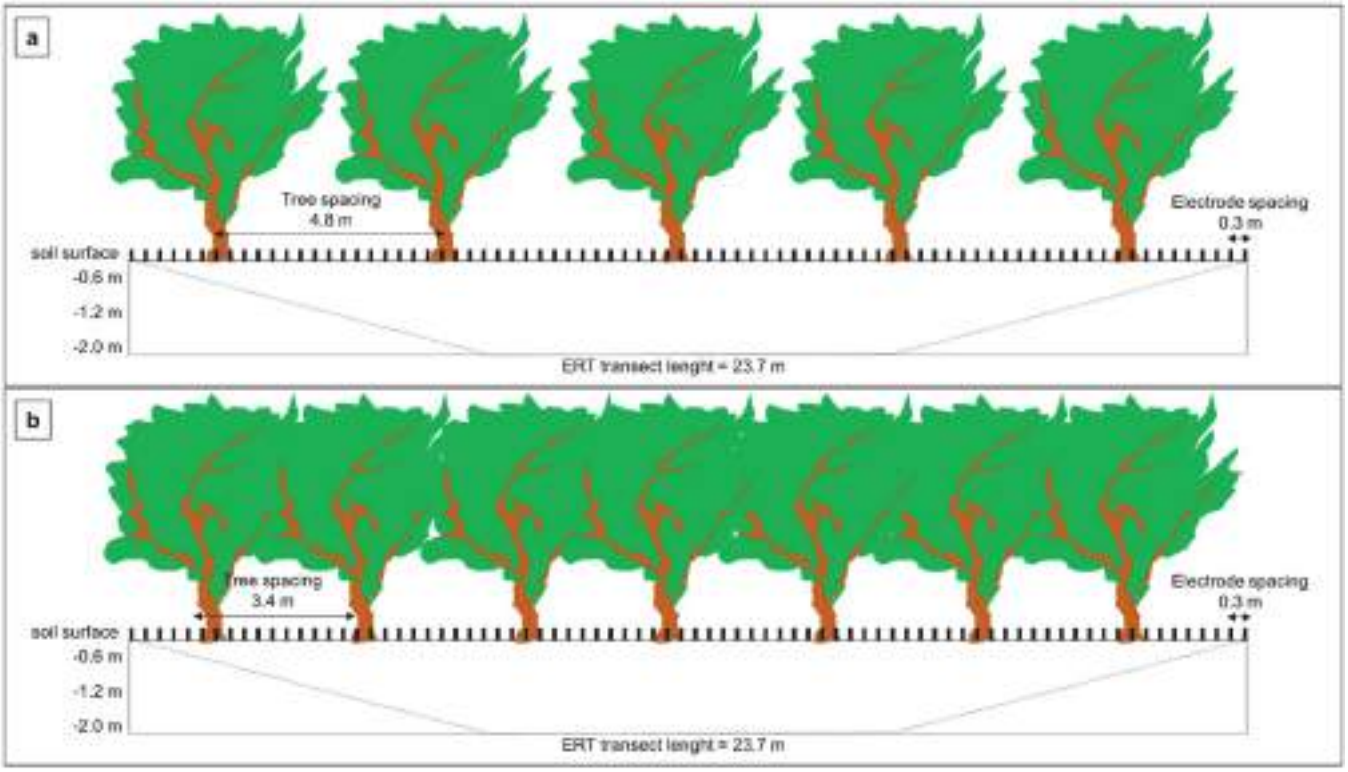

Fig. 2. Electrical resistivity tomography (ERT) layout at the study sites under study: (a) C230#1 and C230#2; and (b) C6#9, C7#12 and C7#14 at the CAPEX ranch located near Corning, California.

2. Methodological approach

In order to achieve the above-mentioned specific objective, the ERT technique was applied at 5 sites located in 3 selected almond orchards (C230, C6 and C7 in Table 1 and Fig. 1), that belonged to a commercial almond ranch called California Almond Packers and Exporters (CAPEX), (http://capexplant.com/), located in the northern part of Sacramento Valley (near Corning, California, USA). The descriptions of the applied measurements methods are described in the following paragraphs 2.1 and 2.2.

The main site-specific soil and plant characteristics of the almond orchards under study are summarized in Table 1.

The crop information (e.g., rootstock and varieties) was provided by the grower. Specifically, Nonpareil-Peach, Butte-Marianna 2624, and Monterey-Peach were the varieties and rootstocks under study in almond orchard blocks C230, C6 and C7, respectively (Table 1). Tree spacing among the rows was 4.8 m in block C230 and 3.4 m in blocks C6 and C7. The row spacing was 6.7 m in all almond orchard blocks.

A first description of the soil information was obtained from the SoilWeb application developed by the California Soil Resource Lab at UC Davis and UC-ANR in collaboration with the USDA Natural Resources Conservation Service (https://casoilresource.lawr.ucdavis.edu/gmap/). Detailed information about soil variability was retrieved by consulting the apparent soil electrical conductivity maps generated for the entire ranch using geophysical non-intrusive methods, such as soil scanning (Veris Technologies, Salina, KS, 67401, Lund et al., 1999) and electromagnetic sensors (EM38, Geonics Limited, Mississauga, Ontario, Canada, L5T 1C6, McNeill, 1992) (Kisekka et al., 2021; Fulton et al., 2011). Fig. 1 shown an overview of the study site, including the 5 study sites selected for carrying out the ERT surveys in the different blocks based on soil management zones (Heavy, Layered and Light soil) identified as above-mentioned in Table 1. In general, these three soil profiles present similar geological origin being characterized by alluvium that has been formed by metamorphic and sedimentary rock formations. The term "Layered soils" refers mainly to the Tehama silt loam soil with fine silty alluvium. The term "Heavy soil" refers to Arbuckle fine loamy soils with alluvium. Then, "Light soils" are Arbuckle gravelly loam with well-drained alluvium. The detailed information about the soil profile characteristics, in terms of textural and hydraulic conductivity information, are given in Table 2.

Irrigation in all the almond orchards was scheduled by the farmer based on stem water potential every week in the period July-August, with irrigation cycle of about 24–48 h split into 2 applications per week in each almond orchard block. Irrigation was applied using a drip irrigation line located close to the tree trunks. The dripper spacing and the flow rate were 0.9 m and 4.4 L h^{-1}, respectively. About 4 and 5 drippers supplied a single almond tree in blocks C230 and C6-C7 locations, respectively. The applied water was measured weekly with inline flow meters. Electrical conductivity (EC) measurements were conducted on 30 water samples (6 samples for site location) using a conductivity meter (Apera Instruments, LLC-AI3719 PC60-Z, Columbus, Ohio, USA) showed low levels of salinity with average and standard deviation values of 224.80 ± 7.83 μS cm^{-1} (at 20 °C).

2.1. Time-lapse electrical resistivity imaging

ERT technique involves several electrodes to measure the ER distribution of the subsurface (Binley and Kemna, 2005). In principle, a pair of electrodes is adopted for injecting current into the soil and another pair is used for measuring the difference in potential, and thus the apparent ER. A set of 4 electrodes is called quadrupole. Given multiple combinations of current and potential electrodes along a transect, a two-dimensional (2-D) image of the real ER can be reconstructed through solving an inverse modeling problem (Binley et al., 2015). A 2-D arrangement of surface electrodes was set-up at the 5 study locations (Fig. 1). Specifically, each ERT array consisted of 80 surface electrodes (stainless steel rods of about 0.30 m, with diameter of 0.01 m) buried for about 1/3 of their length into the soil surface and spaced 0.30 m on the

Table 3
Scheduling of the electrical resistivity tomography (ERT) surveys conducted in the almond orchard blocks C230, C7 and C6 at the CAPEX ranch located near Corning California. The time (hh.mm) is expressed in local time (Greenwich Mean Time 7); t_1-t_6 refer to the time-steps of the ERT dataset collection (*ERT dataset discarded due to battery malfunction).

Almond orchard code	Date (dd-mm-yy)	Dataset time-step	Irrigation status	Starting time (hh.mm)	Ending time (hh.mm)
C230#1	07-12-21	t_0	No irrigation	8.23	8.52
		t_1	During irrigation	10.03	10.30
		t_2		10.37	11.05
		t_3		11.51	12.20
		t_4		13.08	13.36
		t_5		14.41	15.09
		*t_6		16.16	16.46
C230#2	07-19-21	t_0	No irrigation	7.55	8.22
		t_1	During irrigation	9.10	9.37
		t_2		10.05	10.33
		t_3		11.12	11.40
		t_4		12.15	12.45
		t_5		13.28	13.56
		t_6		15.00	15.25
C7#12	07-21-21	t_0	No irrigation	7.48	8.16
		t_1	During irrigation	9.10	9.38
		t_2		10.10	10.38
		t_3		11.15	11.43
		t_4		12.15	12.44
		t_5		13.35	14.03
		t_6		15.00	15.28
C7#14	08-02-21	t_0	No irrigation	7.42	8.10
		t_1	During irrigation	10.39	11.07
		t_2		11.34	12.01
		t_3		12.31	13.00
		t_4		13.23	13.52
		t_5		14.30	15.00
		t_6		15.49	16.17
C6#9	07-28-21	t_0	No irrigation	7.23	7.51
		t_1	During irrigation	8.20	8.48
		t_2		9.24	9.52
		t_3		10.33	11.00
		t_4		11.30	12.00
		t_5		12.52	13.20
		t_6		14.13	14.40

transect. Each ERT transect had a total length of 23.7 m located parallel to the tree rows, covering 4 and 7 trees in almond orchard blocks C230 and C6-C7, respectively (Table 1 and Fig. 2).

A 10 channel Syscal Pro georesistivimeter (IRIS Instruments, Orleans, France) was used for the ERT dataset acquisition. A total of 6006 readings, including both direct and reciprocal quadrupoles (i.e. by swapping potential with current electrodes for each ERT dataset), were collected using a dipole-dipole electrode configuration (with a dipole spacing of 0.30 m), due to its intrinsic strength in solving ER lateral changes (Samoüelian et al., 2005). The high spatial coverage of the adopted ERT array permitted us, adjusting the numbers of measured levels, to reach depths of investigation of about 2 m (Oldenburg and Li, 1999).

The ERT surveys were conducted in time-lapse mode within the period July-August 2021 (Table 3). The time-lapse approach consists of multiple ERT surveys taken at different times during the period of interest (e.g., an irrigation event). In particular, the electrodes (after the initial installation) were left in place at each location allowing the time-lapse ERT measurements to be taken at the same exact position by adopting the following protocol: (i) one ERT dataset acquisition was performed before the beginning of the irrigation event, early in the morning (referred to as t_0 in Table 3), and; (ii) in addition six ERT dataset repetitions were carried out during the irrigation event at different times for the same site location (refer to t_1-t_6, Table 3).

Overall, a total of 30 ERT datasets were acquired during the study period (Table 3) in the almond orchard blocks C230, C7 and C6, (see Table 1). Each ERT dataset collection lasted about 28 min. The electrode galvanic contacts were checked before each ERT dataset acquisition, showing resistance values lower than 5 K Ω.

ERT data processing was performed using the freeware R2 code (v. 4.02, July 2020), which permits the forwarding/inverse solution for two-dimensional (2D) or three-dimensional (3D) current flow in a finite element domain (Binley, 2020). A triangular mesh made of 7016 cells and 13,594 elements was generated using the Gmsh software (Geuzaine and Remacle, 2009). Special attention was paid to the quantification of the measurement and model errors. In particular, measurements with reciprocity error above 10% were removed and these errors were used as weights in the inversion process. In addition, several forward models were run for a uniform resistivity (value fixed at 100 Ω m) in order to sort out the preferred discretization domain (mesh) and evaluating the goodness of the forward model.

The 2-D data inversions were run both in absolute and in time-lapse mode. Specifically, the absolute inverse solution, based on a regularised objective function combined with weighted least squares (an Occam's type solution), was applied as defined in Binley and Kemna (2005) and Binley (2015) for identifying the static ER distribution at the initial conditions (t_0, no irrigation, Table 3) at each site. Conversely to the absolute inversion that accounted for the static effects on soil ER (e.g., from texture), the dynamic ER changes were calculated by implementing the ratio time-lapse inversion following the approach described in Vanella et al. (2021), as follows:

$$\mathbf{d}_r = \frac{\mathbf{d}_t}{\mathbf{d}_0} F(\sigma_{ohm}) \quad (1)$$

where, d_r is the resistance ratio (Ω), d_t and d_0 (Ω) are the resistance dataset collected at selected time periods (t_1–t_7) and at the initial condition (t_0), and $F(\sigma_{ohm})$ is the resistance value (Ω) obtained by running the forward model for a fixed ER value (i.e., 100 Ω m).

According to Eq. (1), the ratio time-lapse inversion approach permits

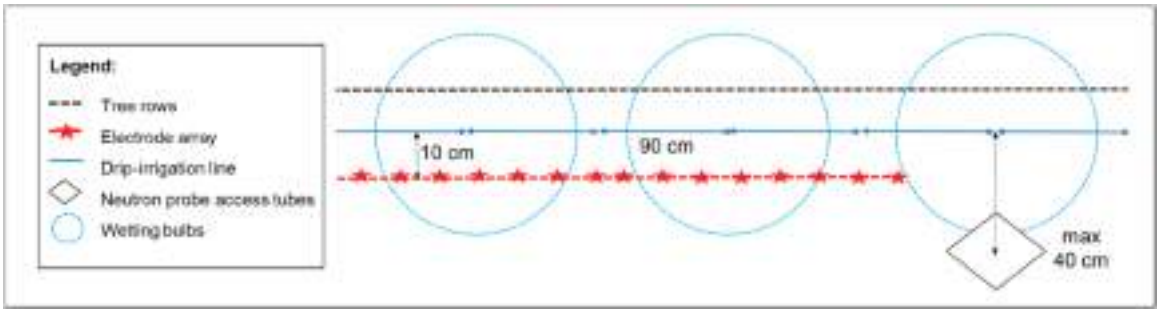

Fig. 3. Location of the neutron probe access tubes in respect to the drip-irrigation line and the electrode array at each site location within CAPEX ranch.

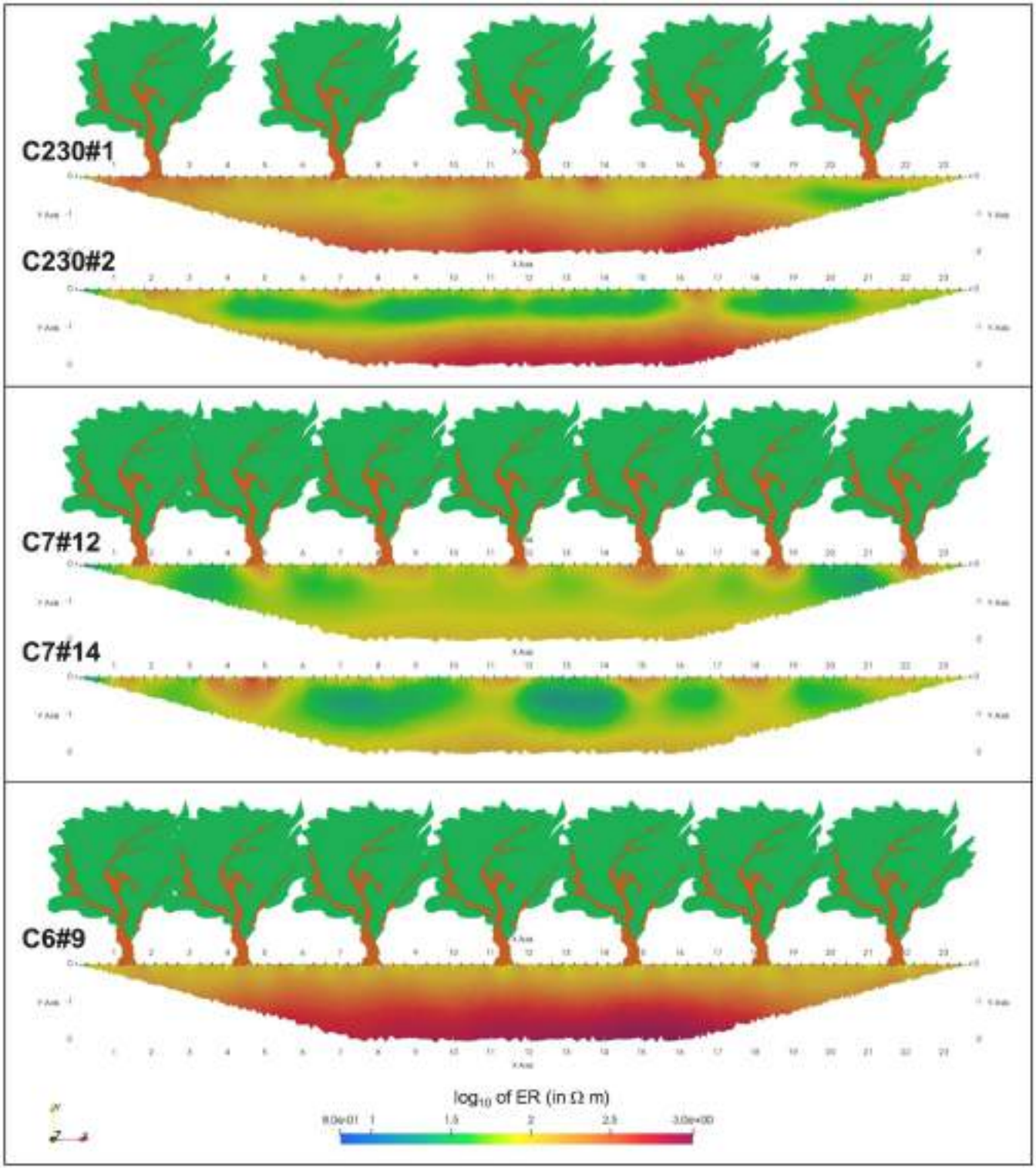

Fig. 4. Electrical resistivity (ER) imagery obtained at study the site locations (C230 #1 and #2, C7 #12 and #14, and C6#9) at the CAPEX ranch almond orchards located near Corning, California. ER data are displayed as $\log_{10}$ of ER (in Ω m) and referred to the initial condition. For interpretation of the references to colour in this figure legend, the reader is referred to the web version of this article.

to recognize the ER changes (%) in comparison to the initial condition (t_0, no irrigation, Table 3) and, thus, to provide evidence for wetting or drying soil patterns (e.g., corresponding to a decline/increase in ER with respect to the reference dataset). The reconstruction of the 2-D ERT imagery was performed using the ParaView software (v. 5.8.1).

2.2. Soil- plant-atmosphere continuum monitoring

2.2.1. Micrometeorological data collection and processing

An eddy covariance flux tower was installed in the middle of CAPEX ranch almond orchards in order to measure the fast and slow surface energy balance (SEB) fluxes exchanged within the soil-plant-atmosphere

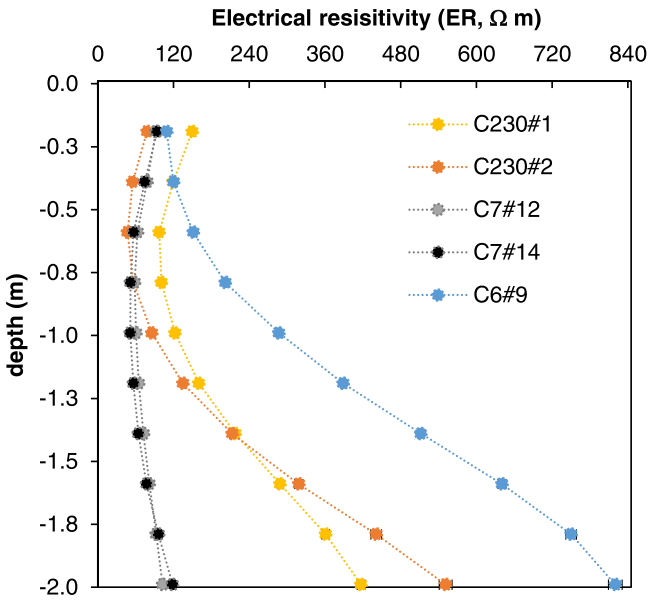

Fig. 5. Average electrical resistivity (ER, Ω m) profiles at the 5 study site locations in the almond orchards of CAPEX ranch located near Corning California in 2021 (C230#1, C230#2, C6#9, C7#12 and C7#14). Bars indicate the standard error values. For interpretation of the references to colour in this figure legend, the reader is referred to the web version of this article.

continuum (Fig. 1). Specifically, the system consisted of a 3D sonic anemometer (Gill R3–50, Li-Cor, USA) and an open-path fast response infrared gas analyzer (LI-7500, Li-Cor Inc., Lincoln, NE, USA), which were placed at a height of 10 m above the ground, for measuring the carbon (CO_2) and water (H_2O) fluxes and for determining the latent heat (LE) and sensible heat (H) fluxes. Additional measurements included the use of a four-component net radiometer (SN-500-SS, Apogee Instruments, Inc, UT, USA) and three soil heat flux plates (HFT-3 from Radiation Energy Balance Systems in Bellevue, WA, USA) for measuring the net radiation (R_n) and the soil heat flux (G), respectively. The soil heat flux plates were buried at a depth of 8 cm and coupled with three soil thermocouples (TCAV-L from Campbell Scientific Inc. in Logan, UT, USA) and soil moisture probes (GS-1, METER Group, Inc. USA), placed at 2.5 cm depth, for correcting the heat storage above them.

Eddy Pro software (v. 7.0.6, Li-Cor, USA) was used for post-processing the turbulent flux data, which included a full range of standard corrections and adjustments, such as the two-dimensional rotation, the spectral corrections (Moncrieff et al., 1997), and the adjustment for the effects of heat and water vapour density fluctuations (Webb et al., 1980). The footprint and data quality analyses were carried out using the TOVI software (Li-Cor, USA). It was found that the energy balance ratio for the study site was 1.67, with an R^2 values of 0.88 observed between the mean turbulent fluxes (H+LE) and the available energy (R_n-G). Readers may refer to Peddinti and Kisekka (2022) for a comprehensive description of the flux tower.

2.2.2. Soil moisture content measurements

Neutron probes are generally used for determining the amount of water within a specific volume of soil at different depths. These probes work by releasing fast neutrons into the soil, where they hit with hydrogen atoms, and generating slow neutrons as a result of the collision. There is a direct relationship between the soil moisture content (SWC) and the number of slow neutrons in the soil. The count of slow neutrons is known as the count rate, and the normalized count rate is generated by dividing the count rate measured at each soil depth by the standard count rate measured on the surface before beginning the measurements. The ratio of these two readings is known as the count ratio (CR).

The SWC was monitored in situ using a neutron probe device (CPN-530 neutron probe - Analytical Technologies Limited, India) mounted on a stand, which was placed over the neutron-probe access tubes located at each study site (Figs. 1and 3). Each neutron-probe access tube reached a depth of 2.9 m from the soil surface, allowing to carry out SWC readings at 10 depths of the soil profile (−0.20, −0.46 −0.76, −1.07, −1.37, −1.68, −1.98, −2.29, −2.59, and −2.90 m). The SWC was analysed in the interval − 0.2 to − 1.98 m according to the depth of investigation of the ERT surveys carried out at the study locations (Fig. 2). The neutron probe readings were acquired according to the ERT time scheduling as reported in Table 3. The standard count value was recorded before each neutron probe survey. All standard count values were taken with the neutron probe sitting on top of its case, which rested on bare dry soil as suggested by Joint FAO/IAEA (2000).

A site-specific calibration equation was applied for estimating the soil moisture content, as follows:

$$\mathrm{SWC} = a \times CR \pm b \quad (2)$$

where SWC is the soil water content, expressed in $m^3\ m^{-3}$; CR is the count ratio; and a and b are fitting parameters varying for different soil types.

To obtain the volumetric water content, independent soil moisture content measurements were conducted in laboratory using the gravimetric method and the bulk density of soil samples collected during the neutron-probe access tubes digging, at a depth up to 3.6 m with 0.3 m intervals (Peddinti et al., 2020). At the same time, neutron count readings were collected. The regression equation was then fitted between CR to the volumetric water content to obtain the calibration equation, which was then used to determine the real SWC (Eq. 2).

2.2.3. Plant water status measurements

Stem water potential (SWP, MPa) measurements were conducted using a pressure chamber (Soilmoisture Equipment Corp., Santa Barbara, California, USA) in order to assess plant water stress and to eventually evaluate deviations from the optimal level of irrigation during the ERT surveys.

One leaf for almond tree (from 5 and 7 trees, at C230 and C6-C7, respectively, Fig. 2), was chosen from the lower shaded canopy and bagged for at least 10 min before it was cut from the tree and placed into the pressure chamber for the SWP measurement. SWP measurements were acquired at several time beginning just prior to irrigation phase and during the irrigation cycle at each study location according to the ERT time-step reported in Table 3. To minimize variability, SWP readings were made by the same operator immediately after the leaf was cut off the tree. As reported by McCutchan and Shackel (1992), bagging the leaf eliminates water loss thus the leaf reaches equilibrium with the water-conducting system of the adjacent branches and trunk. More information about the operation of the pressure chamber for irrigation management in walnut, almond and prune can be found in Fulton et al. (2014). One-way analysis of variance (ANOVA) was carried out on the acquired SWP dataset for assessing the differences among the different time-steps of dataset collection as reported in Table 3. Before performing the ANOVA, we tested the homogeneity of variances of the SWP dataset and we applied the normality test on the basis of Shapiro-Wilk test and quantile-quantile plots. Then, a *post-hoc* analysis based on Tukey HSD test (Tukey Honest Significant Differences) was performed at significance level (p value) of 0.05.

3. Results

3.1. Electrical resistivity distribution

Fig. 4 displays the ERT imagery for the initial condition (no irrigation, Table 3) at the 5 study site locations. As expected, the lighter soil type location at C6#9 showed the highest ER distribution values in

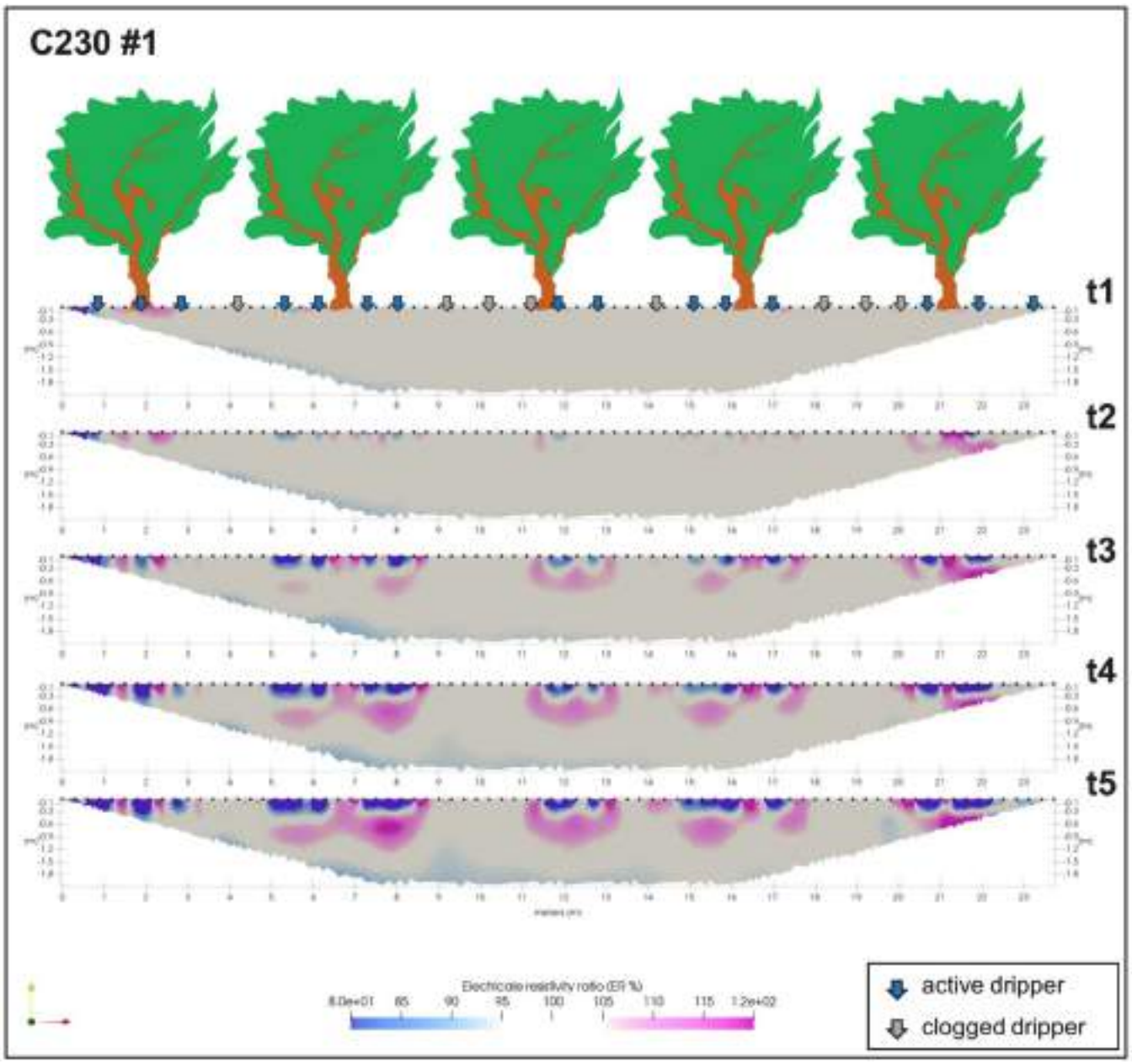

Fig. 6. Electrical resistivity changes (ER, ratio %) observed during different time-steps (t_1-t_5, refer to Table 3) of the irrigation phase in reference to the initial condition (no irrigation) at the C230#1 site at CAPEX ranch located near Corning California. Blue and grey arrows indicate active and partially clogged drippers, respectively. For interpretation of the references to colour in this figure legend, the reader is referred to the web version of this article.

absolute terms, with mean and standard error values of 148.19 and 1.01 Ω m, respectively. Whereas, the lowest ER distribution were observed in the heavier soil locations (C7#12 and C7#14), showing average and standard error values of 74.51 and 0.51 Ω m, respectively. Intermediate ER conditions were detected at C230 location sites (#1 and #2), with mean and standard error values ranging from 104.76 to 148.19 and from 1.01 to 1.40 Ω m, respectively.

The ER average (and standard error) values obtained along the explored soil profiles at the 5 study locations for the initial condition are reported in Fig. 5 as function of depth. Specifically, some ER differences were obtained within the soil profiles at C230 (#1 and #2). Specifically, C230#1 presented higher ER values until 1.4 m of the soil profile than C230#2, showing average ER values of 138.34 and 95.81 Ω m, respectively (and standard error values of 0.54 and 0.77 Ω m, respectively). At the deeper soil layers, ER values tended to be higher in C230#2 than in C230#1, with average values of 436.85 and 355.66 Ω m (and standard error values of 6.63 and 3.66 Ω m, respectively). Unlike study site C230, analogous ER profiles were observed at both study locations #12 and #14 in almond block C7, showing an average standard error of 0.86 Ω m. Overall, all 5 study locations showed an ER increasing trend with depth, though less pronounced at C7 site locations.

3.2. Time-lapse electrical resistivity images

The results of the ERT time-lapse inversions with reference to the "no irrigation" condition are shown in Figs. 6–10. The overall ER changes (%), that are given in Fig. 11, were obtained by averaging the ER changes values (%), referring to the entire ER explored domain, at the different time-steps after the beginning of the irrigation (t_1 – t_6, in Table 3). Specifically, the ERT time-lapse imagery depicted peculiar spatial distribution in terms of ER changes (%) during the different monitoring time-steps (Table 3) at each site location (C230#1–2;

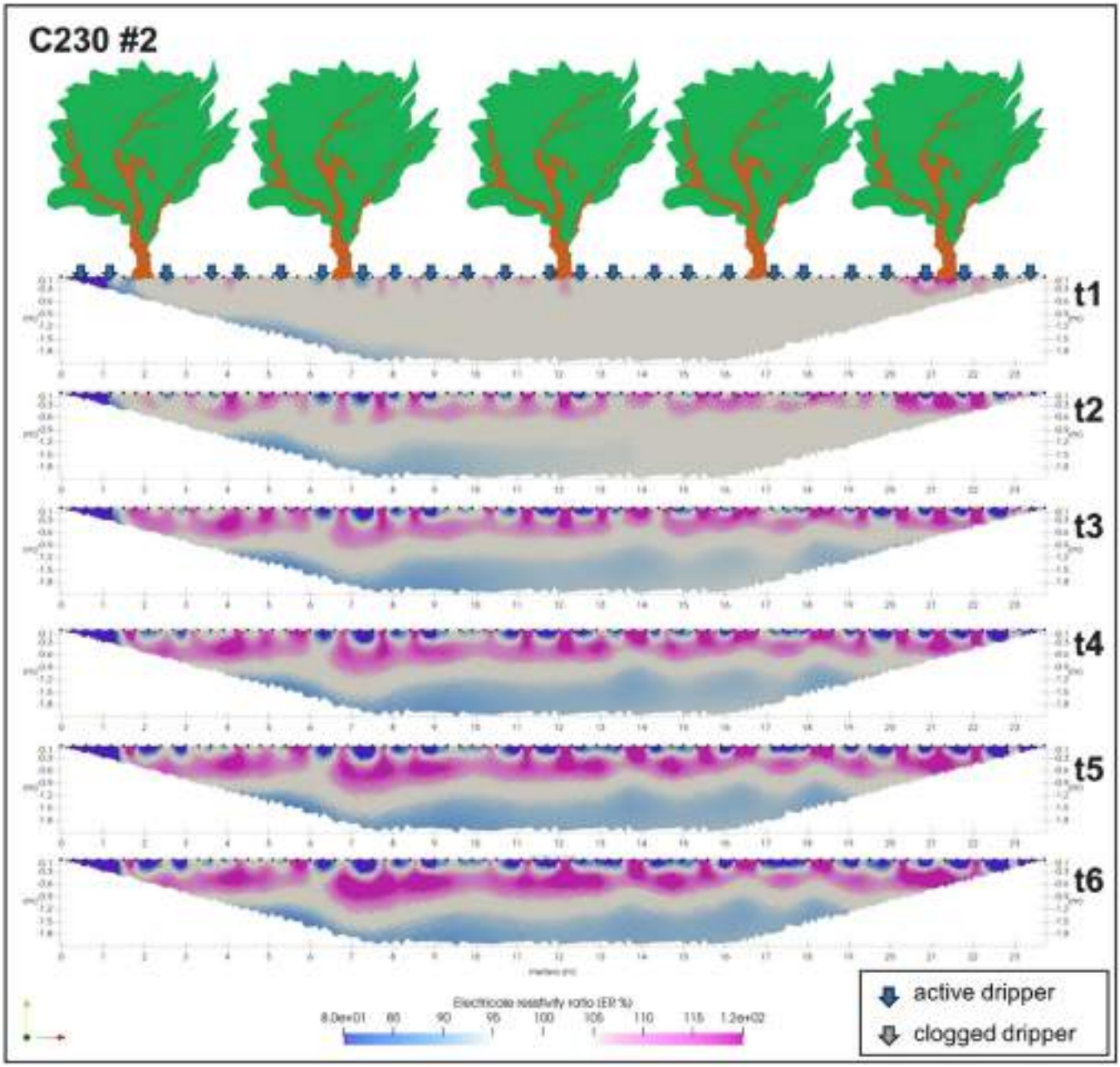

Fig. 7. Electrical resistivity changes (ER, ratio %) during different time-steps (t_1-t_6, refer to Table 3) of the irrigation phase in reference to the initial condition (no irrigation) at the C230#2 site at CAPEX ranch located near Corning California. Blue and grey arrows indicate active and partially clogged drippers, respectively. For interpretation of the references to colour in this figure legend, the reader is referred to the web version of this article.

C7#12–14; and C6#9).

At C230#1, negligible ER changes (0.26% ± 3.60%) were observed at t_1 with respect to the initial condition. Slight ER increasing patterns were observed at t_2 and t_3, corresponding to an overall average increase (± standard deviation) of 0.93% (± 4.84%) and 0.42% (± 8.16%) in terms of ER, respectively. At the same location, localized ER decreasing patterns were retrieved at t_4 and t_5 resulting in an overall ER decrease of − 0.34% (± 10.73%) and − 0.74% (± 12.13%), respectively. As shown in Fig. 6, the ER decreasing patterns were observed until 0.2–0.5 m of the soil depth just under the active drippers (see the blue arrows in Fig. 6). Simultaneously ER increasing patterns were detected both at the soil surface and under the wet bulbs.

A different ER behavior was observed at C230#2 (Fig. 7). In particular, starting from t_2 uniform distributed soil wetting patterns (decreasing in ER) were observed along the subsurface of the ERT transect. These zones corresponded to the propagation of the irrigation wetting fronts, showing stable depths of about 0.2 m from the soil surface at t_2 and being more starting at t_3 until t_6 (reaching a maximum depth of 0.3 m). At the same temporal step, ER increasing patterns (soil drying) were retrieved at the soil surface and under the wet bulbs. These ER increasing patterns tended to be predominant in the investigated subsoil domain, resulting in an overall ER increase of 2.57% (± 13.71%) to 1.73% (± 16.31%) from t_2 to t_4 and from t_5 to t_6, respectively. Similarly, to C230#1, negligible ER changes (−0.10% ± 6.02%) were detected in C230#2 at t_1 corresponding to 47 min after the beginning of the irrigation.

Both study site locations in almond orchard C7 (#12 and #14) showed a similar dominant behavior mainly characterized by average ER increasing, from t_2 to t_6, equal to 2.92% (± 13.60%) and 2.16% (± 18.23%) of the overall investigated domain, respectively (Figs. 8–9).

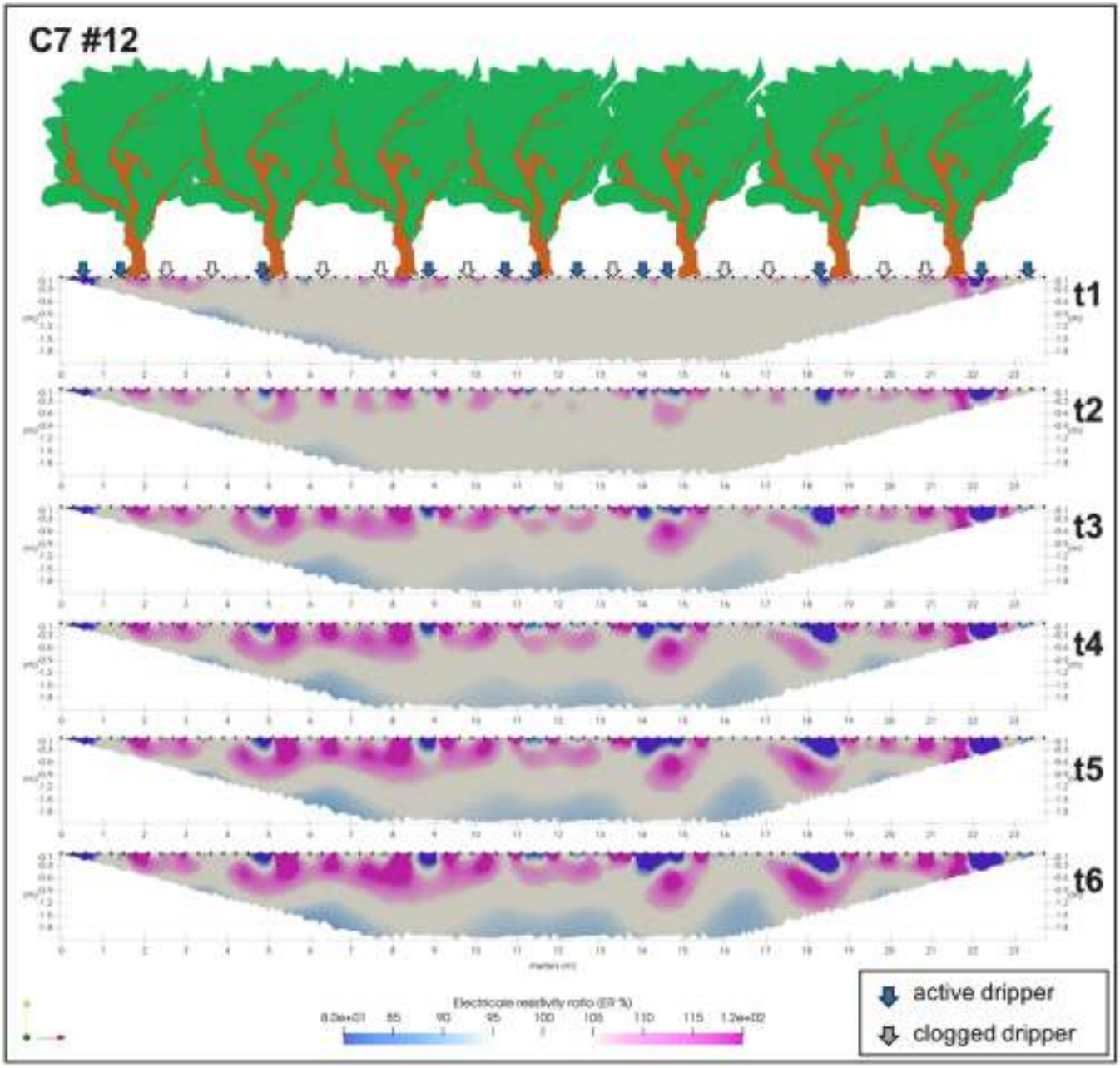

Fig. 8. Electrical resistivity changes (ER, ratio %) during different time-steps (t_1-t_6, refer to Table 3) of the irrigation phase in reference to the initial condition (no irrigation) at the C7#12 site at CAPEX ranch located near Corning California. Blue and grey arrows indicate active and partially clogged drippers, respectively. For interpretation of the references to colour in this figure legend, the reader is referred to the web version of this article.

At t_1 slight increase in ER were observed at both locations, resulting in average changes of 0.75% (± 6.38%) and 0.16% (± 5.82%), respectively. It is interesting to note that both C7#12 and C7#14 were characterized by sporadic preferential ER decreasing patterns (soil wetting), that reached the maximum depth of 0.4 m of the soil profile at t_4 and t_5, respectively. In addition, 1–2 h after the beginning of the irrigation (at t_2 and t_3) both locations were affected by deeper soil drying patterns until − 1.2 m depth of the soil profiles.

Despite the results obtained at the study locations C230 and C7, an evident ER decreasing trend was observed in the subsurface of C6#9 during the ERT time-lapse surveys (Fig. 10). Specifically, a continuous soil wetting pattern was observed from t_1 to t_6, resulting in average ER reductions ranging from − 0.60% (± 4.41%) to − 10.13% (± 9.31%) of the explored domain.

3.3. Soil- plant-atmosphere continuum interactions

3.3.1. Surface energy balance fluxes

The semi-hourly SEB fluxes monitored at the CAPEX site during the study are shown in Fig. 12 together with the indication of the ERT survey time-steps (refer to Table 3). In general, the partitioning of the SEB fluxes measured during the ERT surveys at the 5 site locations show a typical Mediterranean summer trend, with higher values observed for the R_n component, average hourly values observed between 8 a.m. and 4 p.m. varied from 529.67 ± 132.17 W m^{-2} (at C230#1) to 477.32 ± 153.98 W m^{-2} (at C7#14) (without considering the date referred to C230#2 due to the lack of some measurements during the observation period, Fig. 12). The R_n component was followed by the LE term, with average hourly maximum and minimum values recorded at C6#9 (299.99 W m^{-2}) and C7#14 (217.72 W m^{-2}), and then by the H and G

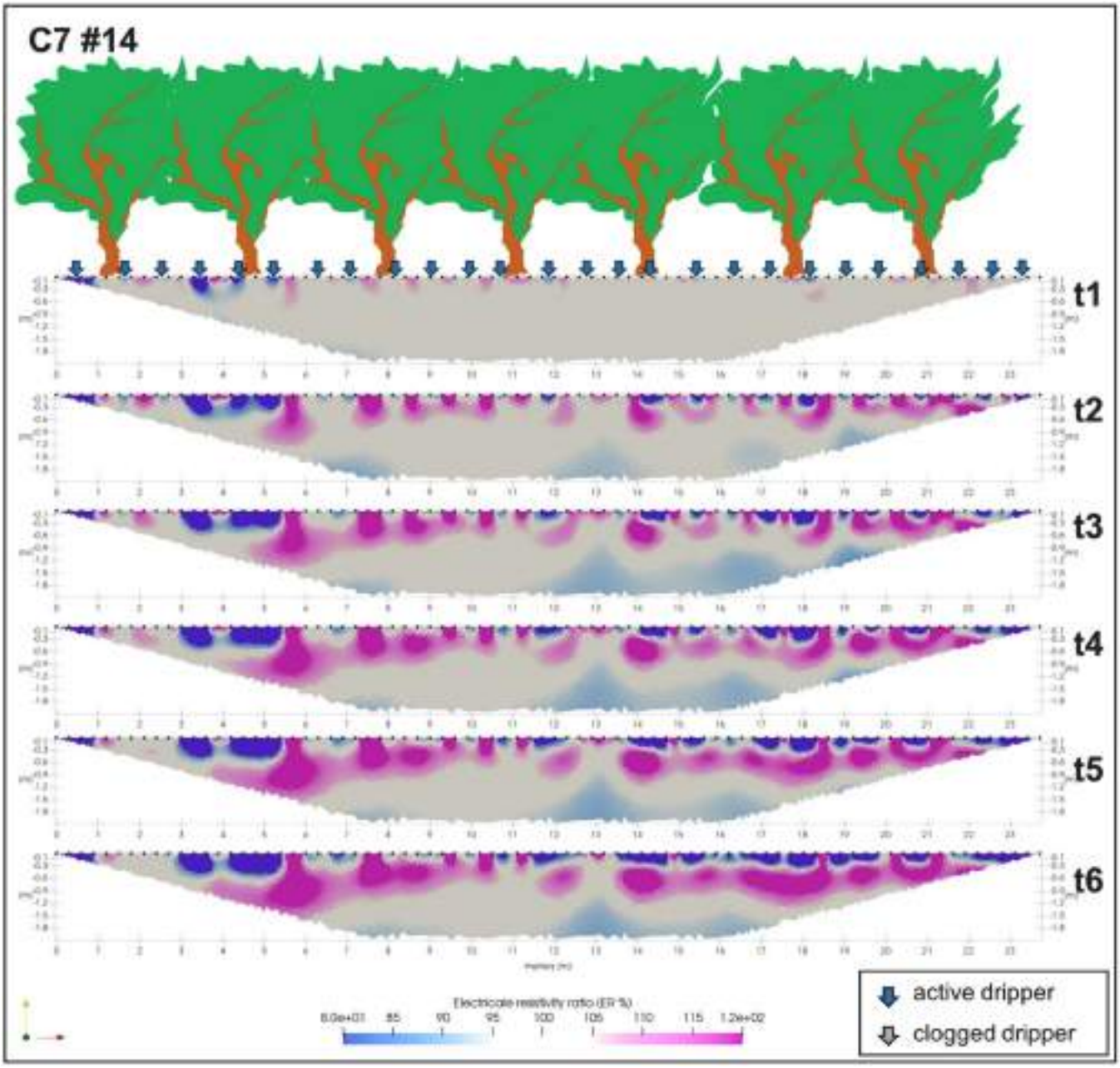

Fig. 9. Electrical resistivity changes (ER, ratio %) during different time-steps (t_1-t_6, refer to Table 3) of the irrigation phase in reference to the initial condition (no irrigation) at the C7#14 site at CAPEX ranch located near Corning California. Blue and grey arrows indicate active and partially clogged drippers, respectively. For interpretation of the references to colour in this figure legend, the reader is referred to the web version of this article.

terms showing the lower values (on average 113.62 ± 39.68 W m^{-2} and 10.82 ± 1.99 W m^{-2}, respectively). The mean hourly actual evapotranspiration (ET) measured at the site locations between 8 a.m. and 4 p.m. was 0.42 ± 0.11 mm h^{-1}, 0.36 ± 0.13 mm h^{-1}, 0.43 ± 0.12 mm h^{-1}, 0.32 ± 0.07 mm h^{-1} and 0.45 ± 0.11 mm h^{-1} for C230#1, C230#2, C7#12, C7#14 and C6#9, respectively.

3.3.2. Soil moisture content profiles

The evolution of the soil moisture content profiles (from 0.2 until 1.98 m depth) monitored at the study site locations (C230#1, C230#1, C7#12, C7#14 e C6#19) during the ERT surveys are shown in Fig. 13. At t_0 (no irrigation), the soil moisture values at C230#1 ranged between 0.20 and 0.35 m^3 m^{-3}, as function of depth. Specifically, an abrupt change in soil moisture was observed between the upper part of the soil profile (within the interval −0.2 and −0.76 m) and the remaining part (within the interval −1.07 and −1.98 m). In particular, the upper part showed greater average (and standard deviation) values of 0.32 ± 0.03 m^3 m^{-3} than the deeper one with average values of 0.21 m^3 m^{-3} (± 0.01). Slight changes were observed in time at C230#1 (from t_1 to t_6) showing soil water reductions of about 7% in the upper part of the soil profile (until a depth of 0.5 m, ranging from 0.33 to 0.31 m^3 m^{-3}) and quite stable lower values (0.23 m^3 m^{-3}) in the deeper layers (> −1 m). At C230#2, the soil moisture condition were variable as function of the soil profile depth, showing values between 0.17 and 0.45 m^3 m^{-3} before the beginning of the irrigation (t_0). In particular, the upper part of the soil profile (until −1.07 m) showed higher soil moisture values equal to 0.38 ± 0.07 m^3 m^{-3}, and lower values (0.20 ± 0.03) in the deeper layers (from −1.37 m until −1.98 m). At this study location, the soil moisture condition did not considerably differ during the irrigation in comparison to the initial one (less than 1%). At C7#12 and C7#14, the

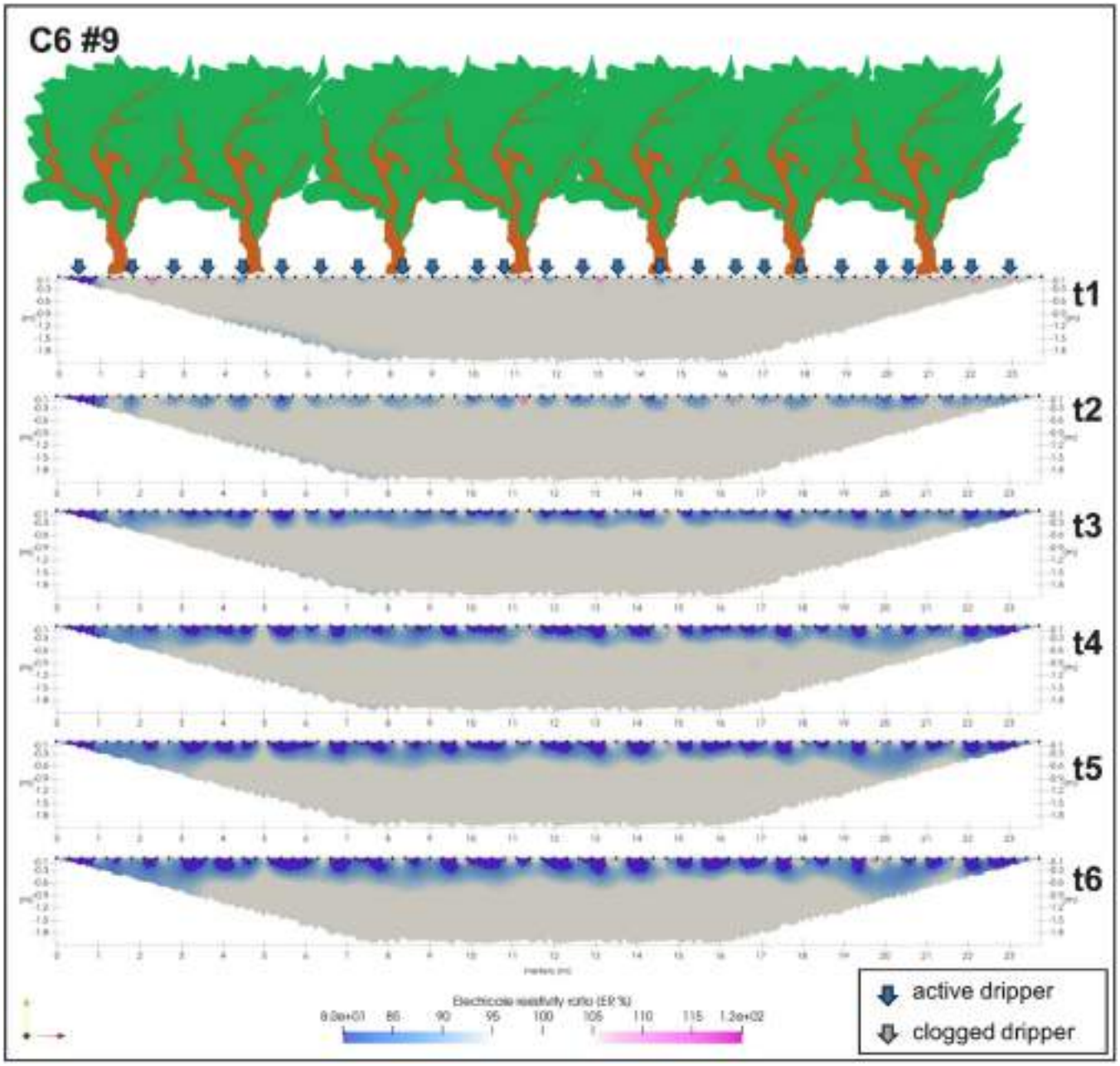

Fig. 10. Electrical resistivity changes (ER, ratio %) during different time-steps (t_1-t_6, refer to Table 3) of the irrigation phase in reference to the initial condition (no irrigation) at the C6#9 site at CAPEX ranch located near Corning California. Blue and grey arrows indicate active and partially clogged drippers, respectively. For interpretation of the references to colour in this figure legend, the reader is referred to the web version of this article.

soil moisture ranged between 0.27 m^3 m^{-3} and 0.39 m^3 m^{-3} and from 0.19 m^3 m^{-3} to 0.35 m^3 m^{-3} at t_0, respectively. Higher values were retrieved at C7#12 at − 0.2 m and from − 1.07 to − 1.37 m depth of the soil profile (in average 0.36 ± 0.04 m^3 m^{-3}). Conversely, at the other depths the soil moisture showed similar values (in average 0.28 ± 0.01 m^3 m^{-3}). In respect to time, the soil moisture at C7#12 tended to decrease by 6% and 3% at − 0.2 m and at − 0.76 m of the soil profile depth after 1–2 h from the irrigation beginning, respectively. Quite stable values with increasing depth of about 1% were observed at − 0.46 m, and from − 1.07 to − 1.37 m of the soil profile. Slight soil moisture increases (about 3%) were detected at the deeper soil layers (from −1.68 to 1.98 m). Unlike C7#12, the intermediate soil layers of C7#14 showed higher soil moisture values (0.33 ± 0.02 m^3 m^{-3}) than the shallower layer (at −0.2 m) and the deeper layers average equaled to 0.20 ± 0.02 m^3 m^{-3} before the irrigation started. At this site, during the irrigation event, the soil moisture changed with a reduction of about 2% in comparison to the initial condition from the shallower layer until − 1.37 m of the soil depth. No changes in soil moisture were observed between − 1.68 and − 1.98 m from the soil surface. The lower soil moisture values at t_0 were registered at C6#9, with values ranging from 0.12 to 0.20 m^3 m^{-3}, that tended to be stable (changes < 1%) during the irrigation phase.

3.3.3. Plant water status patterns

The average SWP (and standard deviation) values ranged from − 1.09 ± 0.08 MPa to − 1.80 ± 0.17 MPa and from − 1.17 ± 0.28 MPa to − 1.84 ± 0.17 MPa at C230#1 and C230#2, respectively; and from − 1.08 ± 0.13 MPa to − 1.71 ± 0.18 MPa and from − 1.46 ± 0.43 MPa to − 2.32 ± 0.41 MPa at C7#12 and C7#14, respectively; and from − 0.74 ± 0.10 MPa to − 1.66 ± 0.17 MPa at C6#9 (Fig. 14).

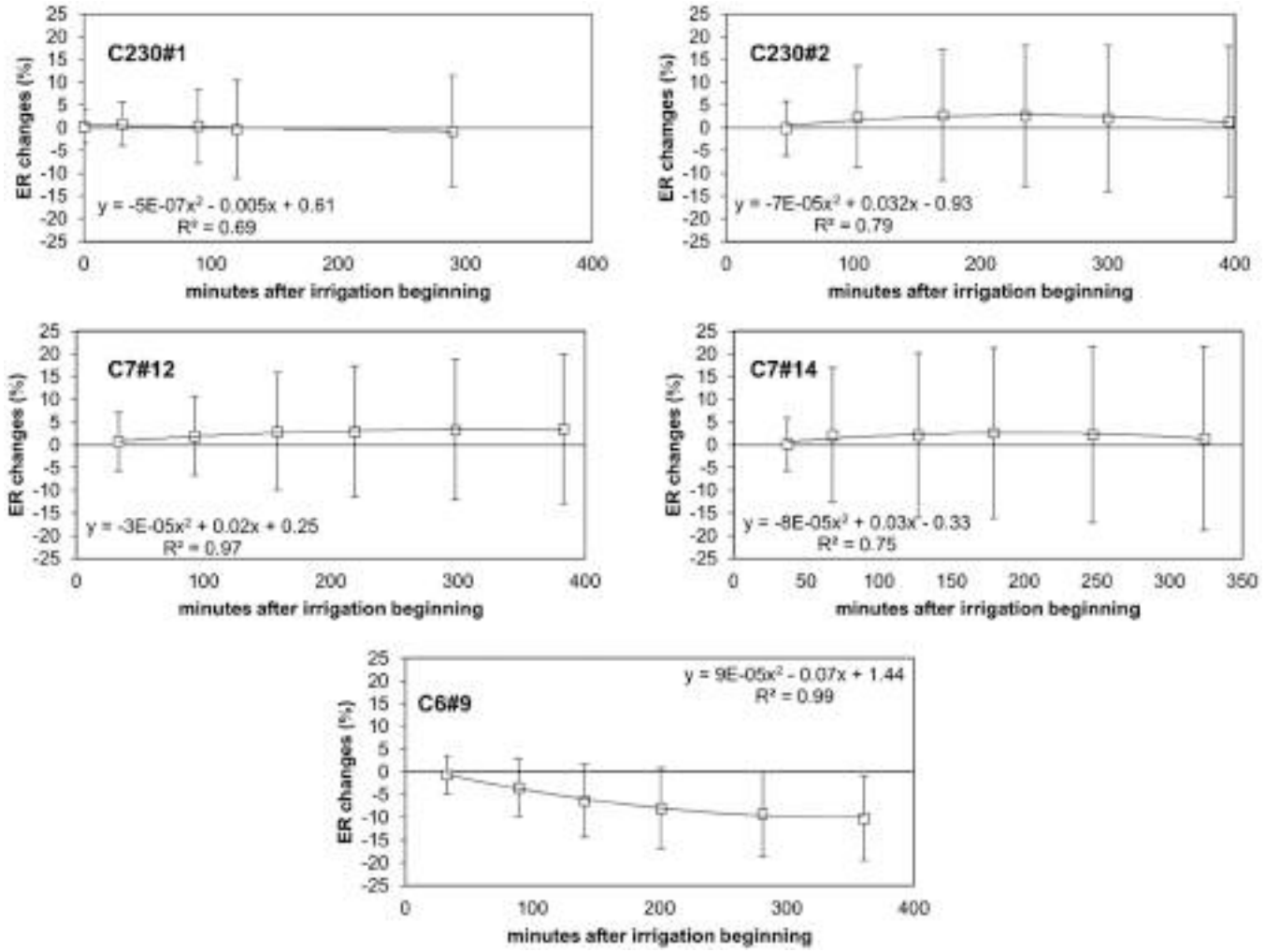

Fig. 11. Overall electrical resistivity changes (ER, %) observed at the study sites during the different time-steps after the beginning of the irrigation phase at the CAPEX ranch located near Corning California. Bars indicate the standard deviation ER changes (%) distribution.

According to the increasing atmospheric demand (Fig. 12), the temporal trend of the SWP values observed within the reference period showed a negative pattern at all the study locations (C230#1, C230#1, C7#12, C7#14 e C6#19) from t_0 to t_6. Specifically, significantly less stressed conditions were identified before the irrigation started (t_0, see Table 3) and more negative SWP values were obtained at the end of the ERT surveys, after about 5 h of irrigation in C230#1 and 6 h at the other site locations. Site-specific SWP variations were also observed during the irrigation phase (i.e. from t_1 to t_3 in C230#1 and from t_1 to t_5 in C230#2, C7#12, C7#14 and C6#9). In particular, even if no differences were retrieved at C230#1 and C230#2, significant differences were obtained at C7#12 and C6#9 between t_1 and t_5. It is interesting to note that from a qualitative point-of-view, definite clusters were identified between the mean SWP and soil moisture neutron-probe values observed during the different time-steps (t_1 - t_5) at the study locations (Fig. 15). Specifically, the maximum ER changes were observed at C6#9 which is characterized by the lighter soil (Table 1) and the lower water content values (Fig. 13) and less negative SWP values (Fig. 14).

4. Discussion

Geophysical surveys have been largely applied for imaging the spatial properties of soil that influence crop productivity (Loke et al., 2013). In some cases, especially for tree crops, the geophysical outputs have been linked to the amount of root biomass (al Hagrey 2007; Rossi et al., 2011) and have permitted a way to provide insights about the root-water-uptake activity (Mary et al., 2018, 2019; Vanella et al., 2018).

Herein, the ER sub-soil distributions at 5 almond orchard sites characterized by soil heterogeneity were explored in order to unravel differences in soil water dynamics both in absolute and in time-lapse terms. Even if the ER measurement and model errors were accounted for the inversion process, permitting us to judge the good quality of the forward model against the good quality of the data, we cannot exclude the eventual presence of inversion artefacts (Clément et al., 2009), especially below 1 m of the soil profile, where the sensitivity was lower, e.g., (see, Supplementary material section).

Different ER sub-soil distributions (in absolute terms) have been observed at the different site locations as function of the soil types under study (Table 1 and Table 2). Specifically, higher and lower ER values were observed in the lighter (C6#9) and heavier soils (C7#12 and C7#14), respectively, with intermediate ER conditions for sites C230#1 and C230#1. This behavior is typical of the unsaturated soils, in which the increase in porosity leads to general increase in the ER of a porous medium (Reynolds, 2011). The ERT observations were in agreement with the neutron probe measurements that showed lower and greater values for C6 (light soil) and C7 (heavy soil) sites, respectively (Fig. 13). In addition, the ERT findings confirmed the goodness of the soil management zones already identified at the CAPEX ranch and the mismatching that existed between the soil unit characterization offered by

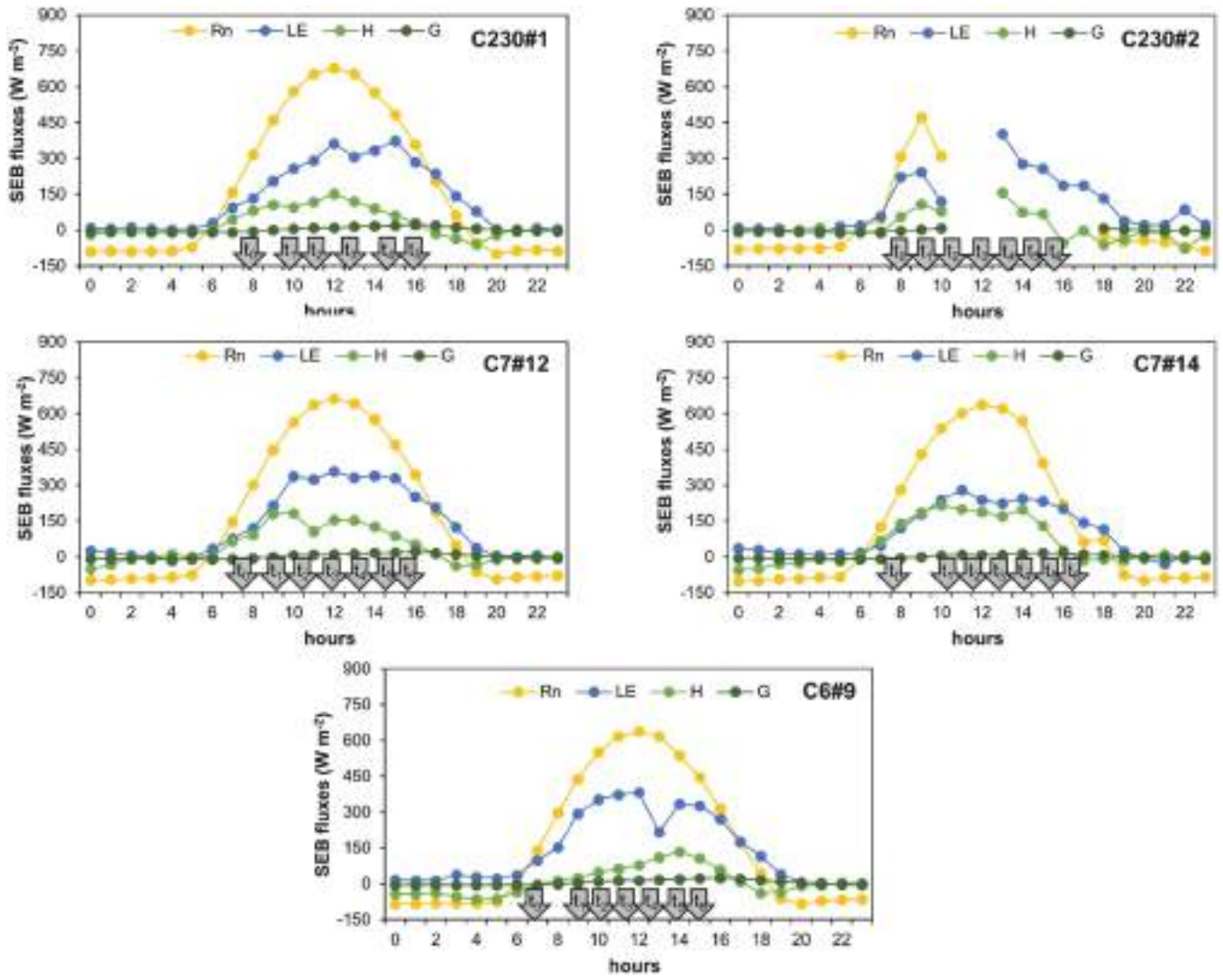

Fig. 12. Hourly surface energy balance fluxes (R_n, LE, H and G refer to the net radiation, latent heat flux, sensible heat flux and soil heat flux, respectively) measured (in W m^{-2}) during the study at the CAPEX ranch located near Corning, California in 2021. The grey arrows indicate the time of the electrical resistivity tomography (ERT) dataset collection (refer to Table 3 for the dataset time steps, t_0-t_6). For interpretation of the references to colour in this figure legend, the reader is referred to the web version of this article.

the SoilWeb (Table 1 and Table 2) and the detailed information provided by the Veris and EM38 technologies (Fulton et al., 2011).

Although the ERT technique can be used for stand-alone survey, time-lapse ERT surveys have shown great potential for agricultural applications, as they enable the observation of the variation of hydrological states that can be related to orchard productivity (Blanchy et al., 2020). Changes in ER have been linked to the variations of soil moisture distribution (Alamry et al., 2017) or soil pore solution concentration (Vanella et al., 2018). Specifically, under our 5 study site locations (Table 1 and Table 2), which took place in a non-saline environment (i.e., Californian Central Valley), the observed ER changes can be reasonably linked to the changes in soil moisture. Specifically, at this non-saline environment, characterized by relatively low EC values of the irrigation water (mean EC values of 224.80 μS cm^{-1} at 20 °C observed during the ERT surveys), it is possible to exclude higher ER contrast with the native soil pore solution concentration. In this sense, we expected that the ER changes are mainly due to the differences in soil structure and texture. These findings are in accordance with Nielson et al. (2021), highlighting the role of time-lapse ERT surveys to infer the soil moisture dynamics as function of the soil structure.

In addition, SWC dynamics inferred by time-lapse ERT surveys were driven by the crop water uptake (or ET, soil drying) and the irrigation process (soil wetting). Similar findings were obtained under micro-irrigation condition both during the irrigation phase and relative redistribution processes (e.g., Ogunmokun and Wallach, 2021, Rahav et al., 2017,Vanella et al., 2021).

It is interesting to note that the magnitude of the ER changes depended on the initial soil moisture content (Vanella et al., 2021). In fact, in our study the greater ER decreasing patterns (Figs. 11 and 15) were detected at the lighter soil study site (C6#9) that showed the lower initial soil moisture content (Fig. 13). The soil wetting inferred by ER changes during the irrigation applications was limited to the 0–40 cm depth interval (Figs. 6–10), which suggests that active root water uptake during the growing season occurred in the shallow soil layer mostly (Koumanov et al., 1997). This evidence suggests also that irrigation infiltration rate was faster than root water uptake at C6#9 (Fig. 15). This hypothesis is supported by the higher hydraulic conductivity values obtained for this soil type (Table 2). Knowledge on the spatial and temporal distribution of soil water status in the root zone during irrigation events is important for efficient water management, especially for microirrigated cropping systems (Koumanov et al., 2006). In general, quantifying the soil moisture in unsaturated environments is difficult

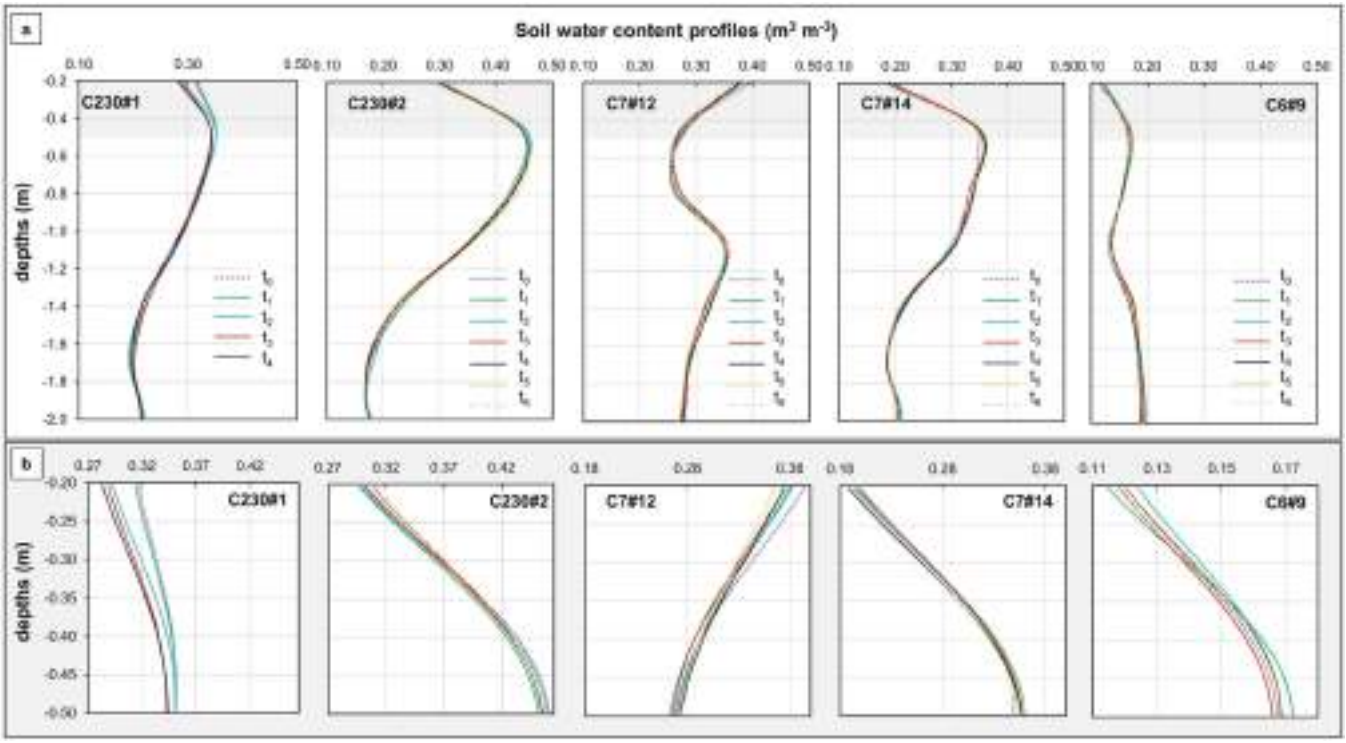

Fig. 13. Soil moisture content ($m^3\ m^{-3}$) profiles monitored using the neutron probe method at the study locations (C230#1, C230#1, C7#12, C7#14 and C6#19) during the electrical resistivity tomography (ERT) surveys at the CAPEX ranch located near Corning California in 2021: (a) overall soil profile until - 2 m depth, and (b) shallow soil profile (from - 0.2 to - 0.5 m depth). For interpretation of the references to colour in this figure legend, the reader is referred to the web version of this article.

due to the complexity of these systems and problems related to the spatially representativeness of the point-based soil moisture measurements (Schwartz et al., 2008), such as the neutron probe method in comparison to plot or field scale methods, being the reliability of the obtained SWC information valid for specific locations and depths (Amiri et al., 2021).

In this study, a weak relationship was obtained between the magnitude of the SWC changes obtained by the neutron probe measurements and the changes inferred by ERT. In particular, slight soil moisture changes were observed by neutron probe measurements at the 5 study site locations during the monitored irrigation events (Fig. 13). This may be due to the offset positions (0.2–0.4 m) of the neutron probe access tubes in respect to the drip-irrigation line (Fig. 3) and to the low performance of the method in operating at shallow soil layers, which could not be detected by the neutron detector and hence resulting in lower than the usual count rate ratios with consequent low SWC (Visvalingam and Tandy, 1972). Assuming that the sampling volume of a neutron probe has a diameter of approximately 0.3 m, this implies that the neutron probe was only sensing a partially wetted volume of soil under micro-irrigation condition. Note that we used existing neutron probe access tubes, that are used for irrigation management when the orchard irrigation system is switched to micro-sprinklers earlier in the season. Generally, the farmer switches to drip irrigation during fertigation and or when water is limited. During the ERT survey, the farmer had switched to drip irrigation due to limited water supplies caused by the drought experienced that year in California.

An advantage of using time-lapse ERT surveys was that they were able to infer the spatially distributed soil moisture changes occurring during the irrigation phases (Figs. 6–10). Our results corroborate the importance of using soil moisture-based techniques (i.e. ERT) in order to improve drip irrigation scheduling and design; and to avoid water deficits and water and fertilizer losses by drainage (Andreu et al., 1997). Simultaneously ER increasing patterns were detected both at the soil surface and under the wet bulbs, showing non-uniform patterns due to the fact that some of the drippers were partially clogged at C230 sites (Figs. 6–7, grey arrows). Moreover, heterogeneity in soil water distribution was assumed by ERT in the mostly heavy soils (C7, in Figs. 8–9). These findings agree with the VERIS maps of bulk soil EC that showed small scale heterogeneities (Kisekka et al., 2021; Fulton et al., 2011). Note also that Figs. 8–9 indicate that the tree root water uptake at the heavy soil profiles occurred at a faster rate in comparison to the rate at which the irrigation was rewetting the soil. This evidence is supported by the high stress conditions, depicted by the higher negative SWP values observed at C7 sites in comparison to the mild stress condition referred to the light soil profile (C6#9) (Figs. 13 and 15). In addition, a supporting explanation of the faster root water uptake than the irrigation infiltration rate occurring under C7 sites is suggested by the lower hydraulic conductivities values associated to these soil types (Table 2). The limitation of the point-based soil moisture measurements has been also reflected in the lack of specific relationships observed between these values and the SWP measurements, even if still some clusters can be identified on the basis of the investigated soil types (Fig. 15). Another explanation of this behavior may be related to the different response timing observed between the soil moisture changes and the plant water status responses. This response time delay can vary according to depth and water content in the soil profile (Grossiord et al., 2018). At the study sites, the hourly temporal evolution of the measured SWP values was more influenced by the ET demand, according to the SEB fluxes measured at the CAPEX ranch (Fig. 12), than by the applied irrigation volume. Specifically, at most of the study locations, hourly SWP differences were maintained constant from 12 p.m. until 4 p.m. (Fig. 14), as observed in other almond orchards under drip irrigation in similar semi-Mediterranean climate (Espadafor et al., 2018). The measurement of SWP under midday conditions (about 1–3 p.m.) is recommended for almond trees (Fulton et al., 2001). In absolute terms, the SWP values described different stress levels, from mild (C6#9) to moderate (C230)

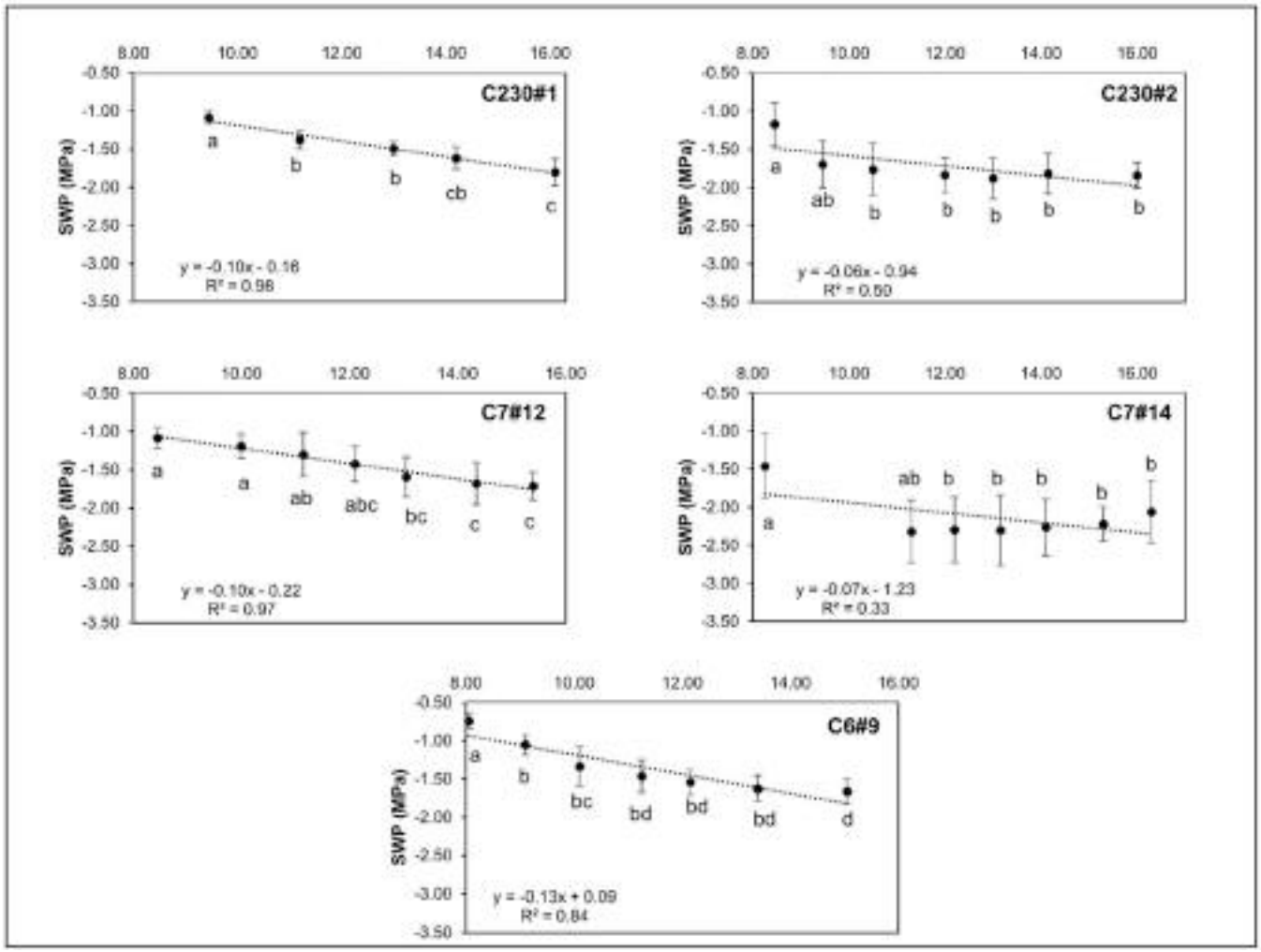

Fig. 14. Average hourly stem water potential (SWP, MPa) values and standard deviation referring to the monitored almond trees at the study locations (C230#1, C230#1, C7#12, C7#14 e C6#19) at the CAPEX ranch located near Corning California. Different letters indicate significant differences according to Tukey's test ($p \leq 0.05$).

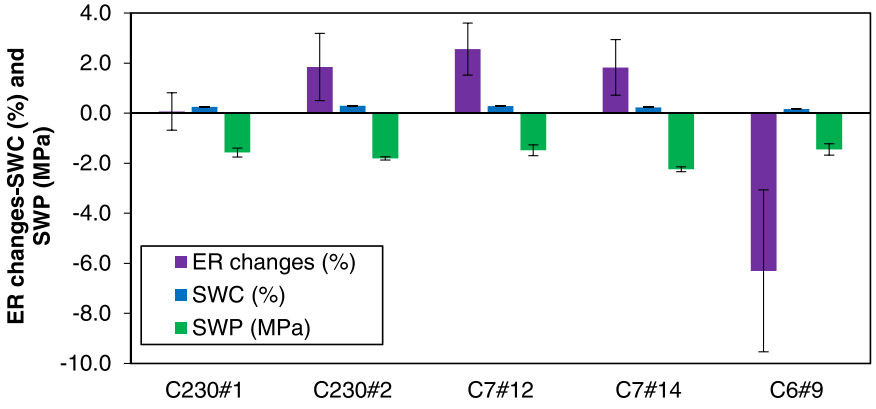

Fig. 15. Average ER changes (%), soil moisture content measured by neutron-probe (SWC, %) and stem water potential (SWP, MPa) values observed during the different time-steps (t_1 - t_5) at the study locations at the CAPEX ranch located near Corning, California. Bars indicate the standard deviation of values. For interpretation of the references to colour in this figure legend, the reader is referred to the web version of this article.

and high (C7#14), at the different study locations, mainly as function of the different soil characteristics varying from lighter to heavier soil and almond varieties and rootstocks (i.e. Nonpareil-Peach, Butte-Marianna 2624, and Monterey-Peach) (Fig. 15).

The maximum total soil water depletion (i.e. ER increasing patterns) were found at the soil surface and under the wetting bulbs (Figs. 6–9) until 1.2 m under the soil surface, due to the combination of the evaporation from the soil and root-water-uptake in the sub-soil processes, respectively. Even if the temporal changes of maximum root water uptake patterns are determined by variations in water availability during

the seasons (Koumanov et al., 2006), our findings are in accordance with Andreu et al. (1997) who estimated that about 65% of the total water uptake occurred in the 0–50 cm depth interval, and that active roots were absent below 1 m soil depth (Fig. 5). This is shown in Fig. 5 in which the effect of soil layering and the irrigation fronts mostly reach the 1 m soil depth.

5. Conclusion

Spatially and temporally distribution of SWC dynamics (i.e., soil drying and wetting patterns) have been inferred by time-lapse ERT surveys conducted during irrigation events under different soil conditions in drip-irrigated almond orchards. This study represents an attempt to interpreter the SWC dynamics, inferred from geophysical data, taking the advantage of integrating multiple measurements about the soil-plant-atmosphere *continuum* system acquired in situ.

In particular, the study highlights the importance of using soil moisture-based techniques (i.e. ERT) to support the irrigation management at the field scale (e.g., for imaging non-uniform wetting patterns due to presence of partially clogged drippers). Moreover, it points out the significance of integrating multiple data to overcome the difficulties of controlling the site-specific parameters affecting the ER behavior under real field conditions (e.g., EC of the irrigation water, soil temperature).

The study puts also in evidence the fact that the interpretation of geophysical data should always be done carefully, e.g., from assuring the data quality to quantifying the adequate weight assignment into the inversion process to providing imagery appraisals.

The derived ER changes were interpreted as *proxy* for exploring the SWC dynamics mainly driven by the soil heterogeneity. The major part of the inferred wet bulb infiltration fronts and root water uptake areas were limited to the upper 0.5 m of the soil profile where the root-systems are supposed to be. These findings help to more accurately estimate the amount of water needed for irrigation, leading to more cost-effective management of the water resource.

Declaration of Competing Interest

The authors declare that they have no known competing financial interests or personal relationships that could have appeared to influence the work reported in this paper.

Acknowledgments

The work was carried out in the frame of Programma Operativo Nazionale (PON) “Attraction and International Mobility” (AIM) 1848200-2 initiative (D.V.). This study was also partially funded by USDA Award # 2021–68012-35914 and Almond Board of California Award # HORT69. We also would like to thank Mr. Robert Mahoney for helping with data collection and the CAPEX management for allowing us to conduct the study on their ranch.

Appendix A. Supporting information

Supplementary data associated with this article can be found in the online version at doi:10.1016/j.agwat.2022.107652.

References

al Hagrey, S., 2007. Geophysical imaging of root-zone, trunk, and moisture heterogeneity. Journal of experimental botany 58 (4), 839–854.

Alamry, A.S., van der Meijde, M., Noomen, M., Addink, E.A., van Benthem, R., de Jong, S.M., 2017. Spatial and temporal monitoring of soil moisture using surface electrical resistivity tomography in Mediterranean soils. Catena 157, 388–396.

Amiri, Z., Gheysari, M., Mosaddeghi, M.R., Amiri, S., Tabatabaei, M.S., 2021. An attempt to find a suitable place for soil moisture sensor in a drip irrigation system. Inf. Process. Agric.

Andreu, L., Hopmans, J.W., Schwankl, L.J., 1997. Spatial and temporal distribution of soil water balance for a drip-irrigated almond tree. Agric. Water Manag. 35 (1–2), 123–146.

Bellvert, J., Mata, M., Vallverdú, X., Paris, C., Marsal, J., 2021. Optimizing precision irrigation of a vineyard to improve water use efficiency and profitability by using a decision-oriented vine water consumption model. Precis. Agric. 22 (2), 319–341.

Binley, A., 2015. Tools and techniques: DC electrical methods. In: Schubert, G. (Ed.), Treatise on geophysics, 2nd ed.,, vol 11. Elsevier, Amsterdam, pp. 233–259. https://doi.org/10.1016/B978-0-444-53802 -4.00192 -5.

Binley, A. (2020) R2 version 3.1 Lancaster University website: ⟨http://www.es.lancs.ac.uk/people/amb/Freeware/R2/R2.htm⟩. Accessed 1 Jul 2021.

Binley, A., Kemna, A., 2005. DC Resistivity and Induced Polarization Methods. In: Rubin, Y., Hubbard, S.S. (Eds.), Hydrogeophysics. Water Science and Technology Library, vol 50. Springer. Dordrecht. https://doi.org/10.1007/1-4020-3102-5_5.

Binley, A., Hubbard, S.S., Huisman, J.A., Revil, A., Robinson, D.A., Singha, K., Slater, L. D., 2015. The emergence of hydrogeophysics for improved understanding of subsurface processes over multiple scales. Water Resour. Res. 51 (6), 3837–3866.

Blanchy, G., Watts, C.W., Richards, J., Bussell, J., Huntenburg, K., Sparkes, D.L., Binley, A., 2020. Time-lapse geophysical assessment of agricultural practices on soil moisture dynamics. Vadose Zone J. 19 (1), e20080.

Cassiani, G., Boaga, J., Vanella, D., Perri, M.T., Consoli, S., 2015. Monitoring and modelling of soil–plant interactions: the joint use of ERT, sap flow and eddy covariance data to characterize the volume of an orange tree root zone. Hydrol. Earth Syst. Sci. 19 (5), 2213–2225.

Clément, R., Descloitres, M., Günther, T., Ribolzi, O., Legchenko, A., 2009. Influence of shallow infiltration on time-lapse ERT: experience of advanced interpretation. Comptes Rendus Geosci. 341 (10–11), 886–898.

De Benedetto, D., Castrignanò, A., Rinaldi, M., Ruggieri, S., Santoro, F., Figorito, B., Gualano, S., Diacono, M., Tamborrino, R., 2013. An approach for delineating homogeneous zones by using multi-sensor data. Geoderma 199, 117–127. https://doi.org/10.1016/j.geoderma.2012.08.028.

Espadafor, M., Orgaz, F., Testi, L., Lorite, I.J., García-Tejera, O., Villalobos, F.J., Fereres, E., 2018. Almond tree response to a change in wetted soil volume under drip irrigation. Agric. Water Manag. 202, 57–65.

Fulton, A., Buchner, R., Gilles, C., Olson, B., Bertagna, N., Walton, J., Shackel, K., 2001. Rapid equilibration of leaf and stem water potential under field conditions in almonds, walnuts, and prunes. HortTechnology 11 (4), 609–615.

Fulton, A., Schwankl, L., Lynn, K., Lampinen, B., Edstrom, J., Prichard, T., 2011. Using EM and VERIS technology to assess land suitability for orchard and vineyard development. Irrig. Sci. 29, 497–512. https://doi.org/10.1007/s00271-010-0253-1.

Fulton, A., Buchner, R., Grant, J. and Connell, J. (2014). Using the Pressure Chamber for Irrigation. Management in Walnut, Almond, and Prune. Oakland: University of California Agriculture and Natural Resources Publication 8503. ANR CS website.

Geuzaine, C., Remacle, J.F., 2009. Gmsh: a three-dimensional finite element mesh generator with built-in pre- and post-processing facilities. Int J. Numer. Methods Eng. 79 (11), 1309–1331.

Grossiord, C., Sevanto, S., Limousin, J.M., Meir, P., Mencuccini, M., Pangle, R.E., McDowell, N.G., 2018. Manipulative experiments demonstrate how long-term soil moisture changes alter controls of plant water use. Environ. Exp. Bot. 152, 19–27.

Joint FAO/IAEA Division of Nuclear Techniques in Food and Agriculture (2000). Comparison of soil water measurement using the neutron scattering, time domain reflectometry and capacitance methods. Results of a consultants meeting (No. IAEA-TECDOC-1137).

Kisekka, I., Fulton, A., Peddinti, S.R., Mahoney, R., 2021. Integrating Soil Moisture, Plant Monitoring, and Imagery for Site-Specific Zone Irrigation Management in Walnuts. Technical Report to the California Water Board. Project # D-0419–28.

Koumanov, K.S., Hopmans, J.W., Schwankl, L.J., Andreu, L., Tuli, A., 1997. Application efficiency of micro-sprinkler irrigation of almond trees. Agric. Water Manag. 34 (3), 247–263.

Koumanov, K.S., Hopmans, J.W., Schwankl, L.W., 2006. Spatial and temporal distribution of root water uptake of an almond tree under microsprinkler irrigation. Irrig. Sci. 24 (4), 267.

Loke, M.H., Chambers, J.E., Rucker, D.F., Kuras, O., Wilkinson, P.B., 2013. Recent developments in the direct-current geoelectrical imaging method. J. Appl. Geophys. 95, 135–156.

Lund, E.D., Christy, C.D., Drummond, P.E., 1999. Practical applications of soil electrical conductivity mapping. July 11–15. In: Stafford, J.V. (Ed.), Precision agriculture ‘99′, Proceedings of the second European conference on precision agriculture. Sheffield Academic Press Ltd., Odense, Denmark, pp. 771–779. July 11–15.

Mary, B., Peruzzo, L., Boaga, J., Schmutz, M., Wu, Y., Hubbard, S.S., Cassiani, G., 2018. Small-scale characterization of vine plant root water uptake via 3-D electrical resistivity tomography and mise-à-la-masse method. Hydrol. Earth Syst. Sci. 22 (10), 5427–5444.

Mary, B., Vanella, D., Consoli, S., Cassiani, G., 2019. Assessing the extent of citrus trees root apparatus under deficit irrigation via multi-method geo-electrical imaging. Sci. Rep. 9 (1), 1–10.

McCutchan, H., Shackel, K.A., 1992. SWP as a sensitive indicator of water stress in prune trees (*Prunus domestica* L.cv French). J. Am. Soc. Hortic. Sci. 117, 607–611.

McNeill, J.D., 1992. Rapid Accurate Mapping Of Soil Salinity By Electromagnetic Ground Conductivity Meters. Advances Of Measurement In Soil Physical Properties: Bringing Theory Into Practice. Special Publication. Soil Science Society of America.

Moncrieff, J.B., Massheder, J.M., De Bruin, H., Elbers, J., Friborg, T., Heusinkveld, B., Kabat, P., Scott, S., Soegaard, H., Verhoef, A., 1997. A system to measure surface fluxes of momentum, sensible heat, water vapour and carbon dioxide. J. Hydrol. 188–189, 589–611. https://doi.org/10.1016/S0022-1694(96)03194-0.

Nielson, T., Bradford, J., Pierce, J., Seyfried, M., 2021. Soil structure and soil moisture dynamics inferred from time-lapse electrical resistivity tomography. CATENA 207, 105553.

Ogunmokun, F.A., Wallach, R., 2021. Remediating the adverse effects of treated wastewater irrigation by repeated on-surface surfactant application. Water Resour. Res. 57 (6) e2020WR029429.

Oldenburg, D.W., Li, Y., 1999. Estimating depth of investigation in dc resistivity and IP surveys. Geophysics 64 (2), 403–416.

Peddinti, S.R., Kisekka, I. (2022). Estimation of turbulent fluxes over almond orchards using high-resolution aerial imagery with one and two-source energy balance models. Agric. Water Manag. (under review).

Peddinti, S.R., Hopmans, J.W., Najm, M.A., Kisekka, I., 2020. Assessing effects of salinity on the performance of a low-cost wireless soil water sensor. Sensors 20, 1–14. https://doi.org/10.3390/s20247041.

Rahav, M., Brindt, N., Yermiyahu, U., Wallach, R., 2017. Induced heterogeneity of soil water content and chemical properties by treated wastewater irrigation and its reclamation by freshwater irrigation. Water Resour. Res. 53 (6), 4756–4774.

Reynolds, J.M. (2011). An Introduction to Applied and Environmental Geophysics; John Wiley and Sons Ltd.: New York, NY, USA.

Rossi, R., Amato, M., Bitella, G., Bochicchio, R., Ferreira Gomes, J.J., Lovelli, S., Favale, P., 2011. Electrical resistivity tomography as a non-destructive method for mapping root biomass in an orchard. Eur. J. Soil Sci. 62 (2), 206–215.

Rudolph, S., van der Kruk, J., von Hebel, C., Ali, M., Herbst, M., Montzka, C., Pätzold, S., Robinson, D., Vereecken, H., 2015. Linking satellite derived LAI patterns with subsoil heterogeneity using large-scale groundbased electromagnetic induction measurements. Geoderma 241–242, 262–271. https://doi.org/10.1016/j.geoderma.2014.11.015.

Samoüelian, A., Cousin, I., Tabbagh, A., Bruand, A., Richard, G., 2005. Electrical resistivity survey in soil science: a review. Soil Res 83, 173–193.

Schwartz, B.F., Schreiber, M.E., Yan, T., 2008. Quantifying field-scale soil moisture using electrical resistivity imaging. J. Hydrol. 362 (3–4), 234–246.

Šimůnek, J., Jarvis, N.J., M.Th. van Genuchten, Gardenas, A., 2003. Review and comparison of models for describing non-equilibrium and preferential flow and transport in the vadose zone. J. Hydrol. 272, 14–35. https://doi.org/10.1016/S0022-1694(02)00252-4.

Vanella, D., Cassiani, G., Busato, L., Boaga, J., Barbagallo, S., Binley, A., Consoli, S., 2018. Use of small scale electrical resistivity tomography to identify soil-root interactions during deficit irrigation. J. Hydrol. 556, 310–324.

Vanella, D., Ramírez-Cuesta, J.M., Intrigliolo, D.S., Consoli, S., 2019. Combining electrical resistivity tomography and satellite images for improving evapotranspiration estimates of citrus orchards. Remote Sens. 11 (4), 373.

Vanella, D., Ramírez-Cuesta, J.M., Sacco, A., Longo-Minnolo, G., Cirelli, G.L., Consoli, S., 2021. Electrical resistivity imaging for monitoring soil water motion patterns under different drip irrigation scenarios. Irrig. Sci. 39 (1), 145–157.

Vereecken, H., Huisman, J.A., Bogena, H., Vanderborght, J., Vrugt, J.A., Hopmans, J.W., 2008. On the value of soil moisture measurements in vadose zone hydrology: a review. Water Resour. Res. 44. https://doi.org/10.1029/2008WR006829.

Vereecken, H., Weihermüller, L., Jonard, F., Montzka, C., 2012. Characterization of crop canopies and water stress related phenomena using microwave remote sensing methods: A review. Vadose Zone J. 11. https://doi.org/10.2136/vzj2011.0138ra.

Vereecken, H., Schnepf, A., Hopmans, J.W., Javaux, M., Or, D., Roose, T., Young, I.M., 2016. Modeling soil processes: review, key challenges, and new perspectives. Vadose zone J. 15 (5).

Visvalingam, M., Tandy, J.D., 1972. The neutron method for measuring soil moisture content - a review. J. Soil Sci. 23 (4), 499–511.

Webb, E.K., Pearman, G.I., Leuning, R., 1980. Correction of flux measurements for density effects due to heat and water vapour transfer. Q. J. R. Meteorol. Soc. 106, 85–100. https://doi.org/10.1002/qj.49710644707.